

Gate-free state preparation for fast variational quantum eigensolver simulations: ctrl-VQE

Oinam Romesh Meitei,^{1,*} Bryan T. Gard,^{2,*} George S. Barron,² David P. Pappas,^{3,4} Sophia E. Economou,² Edwin Barnes,² and Nicholas J. Mayhall^{1,†}

¹*Department of Chemistry, Virginia Tech, Blacksburg, VA 24061, USA*

²*Department of Physics, Virginia Tech, Blacksburg, VA 24061, USA*

³*Physics Department, University of Colorado, Boulder, CO 80309*

⁴*National Institute of Standards and Technology, Boulder, CO 80305*

The variational quantum eigensolver (VQE) is currently the flagship algorithm for solving electronic structure problems on near-term quantum computers. This hybrid quantum/classical algorithm involves implementing a sequence of parameterized gates on quantum hardware to generate a target quantum state, and then measuring the expectation value of the molecular Hamiltonian. Due to finite coherence times and frequent gate errors, the number of gates that can be implemented remains limited on the current state of the art quantum devices, preventing accurate applications to systems with significant entanglement, such as strongly correlated molecules. In this work, we propose an alternative algorithm (which we refer to as **ctrl-VQE**) where the quantum circuit used for state preparation is removed entirely, replaced by a quantum control routine which variationally shapes a pulse to drive the initial Hartree-Fock state to the full CI target state. As with VQE, the objective function optimized is the expectation value of the qubit-mapped molecular Hamiltonian. However, by removing the quantum circuit, the coherence times required for state preparation can be drastically reduced by directly optimizing the pulses. We demonstrate the potential of this method numerically by directly optimizing pulse shapes which accurately model the dissociation curves of the hydrogen molecule (covalent bond) and helium hydride ion (ionic bond).

I. INTRODUCTION

Molecular modeling stands in the juncture of key advances in many important fields including and not limited to energy storage, novel material designs, and drug discovery. For more than half a century, many seminal works have been reported on the development of theories and methods to enable molecular modeling with high accuracies. Approximate numerical methods which are built on a single Slater determinant reference state, such as density functional theory (DFT), perturbation theory, or coupled cluster, perform well when the amount of electron correlation, ranges from minimal to moderate. However, for systems which are qualitatively governed by electron correlation effects (strongly correlated systems), such approximate methods fail to be sufficiently accurate. While alternative strategies exist, such as density matrix renormalization group (DMRG)^{1–3} or selected configurational interaction (SCI) methods,^{4–13} which can handle strong correlation, these approaches assume that the correlations are either low-dimensional, or limited in scale. Currently, no polynomially scaling classical algorithm exists which can solve for arbitrary molecular ground states.

High dimensionality of the wavefunction is ultimately the core reason for the exponential cost of modeling electronic structure. Even before optimization, simply storing the wavefunction on classical hardware quickly becomes a bottleneck. This is because one typically represents the wavefunction in a basis of “classical” states, or basis states which have a direct product structure (Slater determinants, occupation number vectors, or even tensor product states¹⁴). In this classical basis, the exact (and generally entangled) state of the system is represented as

an exponentially⁶⁵ large vector of coefficients weighting the corresponding classical basis states.

Quantum computing offers a radical departure from this computational strategy. As quantum systems themselves, the state of a quantum processing unit (QPU) is also a vector in a Hilbert space of identical dimension to the molecular problem. This ability to perform a one-to-one mapping between vectors in the Hilbert space containing the molecule’s electronic wavefunction and those in the state space accessible to a QPU means that with enough control over the QPU, it should be possible to take the vector corresponding to the molecular wavefunction and realize it on the QPU, avoiding altogether the requirement to work with an exponentially large vector of coefficients. Once the QPU is prepared into the state corresponding to the target molecule, any molecular observable (energy, dipole moment, etc) can be obtained by measuring the corresponding operator on the QPU.

In order to turn this strategy into an algorithm, one needs a procedure for realizing the target molecular wavefunction on the QPU. As the leading quantum algorithm for molecular simulation, the Variational Quantum Eigensolver (VQE)¹⁵ provides an efficient procedure for this purpose. In VQE, one defines a parameterized quantum circuit comprised of tunable gates, and then optimizes these gates using the variational principle, minimizing the energy of the molecular Hamiltonian. This parameterized quantum circuit (referred to as an ansatz) defines the variational flexibility (and thus the subspace reachable on the QPU) of the algorithm.

State-preparation circuits with more parameters generally have more variational flexibility, but come with the cost of having deeper quantum circuits and more dif-

difficult optimization. This cost can be significant. Current and near-term quantum computers are classified as noisy intermediate scale quantum (NISQ) devices due to the presence of short coherence times, system noise, and frequent gate errors. Because each gate has limited fidelity, the success probability for a sequence of gates decreases exponentially with circuit depth. This limits the number of gates that one can apply in a circuit which, in turn, limits the accuracy of the molecular VQE simulation. Although VQE is relatively robust in the presence of noise and errors in certain cases¹⁶, the critical limitation preventing larger scale experiments is the accurate implementation of deep circuits. The goal of finding parameterized circuits which minimize the circuit depth and maximize the accuracy has led to a number of approaches such as hardware efficient ansätze,¹⁷ physically motivated fixed ansätze,^{18–22} and adaptive ansätze.^{23–25}

In this paper, we explore the possibility of performing gate-free VQE simulations by replacing the parameterized quantum circuit with a direct optimization of the laboratory-frame analogue control settings. In the following sections, we argue that quantum control techniques are likely to be better suited for fast VQE state preparation than the more conventional circuit-based approaches on NISQ devices. We first provide a detailed overview of circuit based VQE, then introduce our proposed strategy, `ctrl-VQE`, then discuss initial results, and finally compare to gate-based ansätze. Several technical aspects, numerical results along with discussions noted in this manuscript are provided in the supplementary information.

II. METHOD

A. Variational Quantum Eigensolver

The variational quantum eigensolver (VQE) algorithm aims to leverage classical resources to reduce the circuit depth required for molecular simulation. The algorithm finds optimal rotation angles for a parameterized quantum circuit of fixed depth by variationally minimizing the target molecule’s energy, which is obtained by repeated state preparation and measurement cycles. In order to account for the distinguishability of qubits, we start by transforming the second quantized electronic Hamiltonian into an equivalent form involving non-local strings of Pauli spin operators, \hat{o}_i .

$$\begin{aligned} \hat{H}^{\text{molecule}} &= \sum_{pq} h_{pq} \hat{p}^\dagger \hat{q} + \frac{1}{2} \sum_{pqrs} \langle pq|rs \rangle \hat{p}^\dagger \hat{q}^\dagger \hat{s} \hat{r} \\ &= \sum_i \hat{o}_i h_i, \end{aligned} \quad (1)$$

where h_i is the resulting coefficient which is a sum of molecular one or two-electron integrals. Several such transformations exist, such as the Jordan-Wigner, Bravyi-Kitaev, or parity transformation.^{26–28} In this

work which focuses on two-electron problems, we use the parity transformation and reduce the number of active qubits from four to two. The main steps in VQE are defined as follows:

1. Precompute all h_i values, and transform terms in the Hamiltonian operator into the desired qubit representation.
 2. Choose an ansatz for the problem which defines the variables ($\vec{\theta}$) to optimize. Assuming one starts from the Hartree-Fock reference state, this involves predefining a parameterized circuit which provides enough variational flexibility to describe the molecule’s electron correlation effects. Many ansätze have been proposed, several of which are variants of the original proposal using the Unitary Coupled-Cluster (UCC) ansatz.^{29,30}
 3. Choose an initial set of parameter values, $\vec{\theta} = \vec{\theta}_0$. These can be initialized to zero, chosen randomly, or if appropriate, chosen based on some classical precomputation such as using MP2 parameters to start a UCCSD optimization.
 4. Using current parameters, $\vec{\theta}$, repeatedly execute the circuit, each time performing an individual measurement of one of the operators, \hat{o}_i , in \hat{H} .⁶⁶ After a sufficient number of circuit executions (shots), the averages of the resulting data converges to the expectation values of the operators such that the average molecular energy can be obtained by multiplication with the one and two-electron integrals,
- $$E(\vec{\theta}) = \sum_i h_i \langle \psi(\vec{\theta}) | \hat{o}_i | \psi(\vec{\theta}) \rangle. \quad (2)$$
5. Check convergence. If the average energy has decreased by a small enough value determined to be converged, exit. If the energy is not yet converged, update $\vec{\theta}$, and return to step 4.

Various approaches have been proposed, each differing in the details of state-preparation,^{24,31–35} and ways to reduce the number of circuits required to compute expectation values^{36–39}.

B. Control Variational Quantum Eigensolver: `ctrl-VQE`

In this section, we present an alternative to the gate-based VQE algorithm, replacing the parameterized state-preparation circuit with a parameterized laboratory-frame pulse representation, which is optimized in an analogous manner, but with the benefit of a much faster state preparation, opening up more accurate simulations on near-term devices with short coherence times. All other

aspects of VQE (i.e., measurement protocols) are essentially the same. Using the molecular energy as the objective function to minimize, the pulse parameters are optimized using the variational principle. This general strategy, which we refer to as control variational quantum eigensolver (**ctrl-VQE**), is outlined as follows:

1. As done in any regular VQE, compute the one- and two- electron integrals and transform the molecular Hamiltonian into a qubit representation, for example using Jordan-Wigner, Parity or Bravyi-Kitaev mappings. This defines the objective function to minimize, $\min \langle \hat{H}^{\text{molecule}} \rangle$.
2. Define a fixed pulse representation (e.g. square pulses, sum of Gaussian pulses, etc.). Parametrize the chosen pulse representation, and initialize parameters.
3. Choose an initial state for the qubit(s) system. Hartree Fock is a good choice for the molecular problems studied here. Controls are assumed to be in the form of direct drives on each qubit.
4. Measure the expectation value of the objective function $\langle \hat{H}^{\text{molecule}} \rangle$ on the quantum device.
5. Using a classical optimization routine, determine the pulse parameters for the next measurement on the quantum device.
6. Repeat until a target convergence threshold is met. If the chosen parameterized pulse can fully specify the target Hilbert space, then the optimal pulse finds the minimum energy state.

We note here that the optimization used in this work excludes the total pulse duration. This is fixed throughout the optimization routine, and only the pulse parameters such as the amplitudes or the frequencies are directly optimized. As such, the total pulse time enters the algorithm as a “hyper-parameter”, which can be optimized in an outerloop if desired. In the square pulses considered in this work, the time segments are also optimized. As such, unless stated otherwise, optimal pulses correspond to pulse shapes that are optimal with a given fixed total pulse duration.

Unlike universal quantum computing algorithms, **ctrl-VQE** occurs at the hardware-level, and any simulation must refer to a specific platform. For this work, we choose a well-established transmon platform with the following device Hamiltonian⁴⁰:

$$\hat{H}_D = \sum_{k=1}^2 \left(\omega_k \hat{a}_k^\dagger \hat{a}_k - \frac{\delta_k}{2} \hat{a}_k^\dagger \hat{a}_k^\dagger \hat{a}_k \hat{a}_k \right) + g(\hat{a}_1^\dagger \hat{a}_2 + \hat{a}_2^\dagger \hat{a}_1). \quad (3)$$

This system has two, “always on” directly coupled transmons, where \hat{a}_k is the bosonic annihilation operator for

the k^{th} transmon, and ω_k , δ_k , and g are the resonant frequency, anharmonicity, and constant coupling rate, respectively. Furthermore, each transmon in Eq. (3) formally supports an infinite number of states. However, in our simulations we necessarily approximate this system to a finite number of levels (three unless otherwise stated) per transmon. We tested the accuracy of this by adding more levels and found that the results didn’t significantly change. The parameters used in this work are chosen to be typical parameter values used in current superconducting transmons, and are provided in Table I. We find that our results below do not qualitatively depend on the frequency difference between the qubits, and in the supplementary material we provide a comparison of this current device to one with a larger detuning between the transmons. In order to drive the device, we apply a time dependent field, with separate controls on each qubit such that within the rotating wave approximation, the control Hamiltonian is expressed as:

$$\hat{H}_C = \sum_{k=1}^2 \Omega_k(t) (e^{i\nu_k t} \hat{a}_k + e^{-i\nu_k t} \hat{a}_k^\dagger). \quad (4)$$

where $\Omega_k(t)$ is the real-valued, time-dependent amplitude of the drive, and ν_k is the frequency of the field. The system therefore evolves under the total Hamiltonian:

$$\hat{H} = \hat{H}_D + \hat{H}_C(t, \Omega_n(t), \nu_n). \quad (5)$$

By moving to the interacting frame, the final ansatz has the following form:

$$|\psi^{\text{trial}}(\Omega_n(t), \nu_n)\rangle = \mathcal{T} e^{-i \int_0^T dt \hat{H}_C(t, \Omega_n(t), \nu_n)} |\psi_0\rangle. \quad (6)$$

where $|\psi_0\rangle$ is the VQE reference state (e.g., Hartree-Fock state), $\{\Omega_n(t), \nu_n\}$ are the variational parameters for the ansatz, T is the total pulse time, and \mathcal{T} is the time-ordering operator. Note that although the control Hamiltonian above only has single-qubit terms, the device itself has inter-qubit couplings (Eq. 3 with strength g), which create an entangling control Hamiltonian in the interacting frame:

$$\hat{\hat{H}}(t)_C = e^{i\hat{H}_D t} \hat{H}_C(t) e^{-i\hat{H}_D t}. \quad (7)$$

As such, the coupling strength g is ultimately responsible for describing electron correlation in the target molecule.

Using this ansatz in Eq. 6, the energy to be minimized in the **ctrl-VQE** objective function is,

$$E(\Omega_n(t), \nu_n) = \langle \psi^{\text{trial}} | \hat{H}^{\text{molecule}} | \psi^{\text{trial}} \rangle \quad (8)$$

where $|\psi^{\text{trial}}\rangle$ is just the $|\psi^{\text{trial}}\rangle$ state above, projected onto the computational basis and normalized. Note, that an unnormalized state can also be used, yielding similar results, with examples provided in the SI.

The ansatz above is completely (and solely) determined by the device and controls, granting enormous flexibility to the ansatz. In fact, any digital quantum circuit

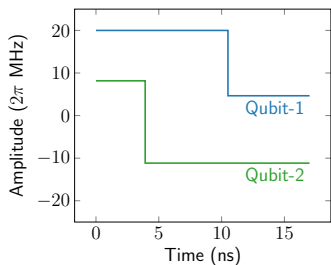


FIG. 1: Illustration of a simple square pulse with two time segments used in this work.

ansatz can be compiled into the form above. As such, the ansatz in Eq. 6 does not intrinsically possess any limitation on its potential accuracy beyond the fundamental limitations imposed by quantum speed limits.⁴¹ However, this additional flexibility can make optimization more difficult. In this work, we have chosen to impose simple constraints on the form of $\Omega_n(t)$, to simplify optimization. We have considered two examples: i) piecewise-constant pulses, and ii) sum of Gaussian pulses. Because these two examples yield similar results, we present only the square pulse data in the main text, and provide the Gaussian pulse data in the Supplementary material. For the piecewise constant pulses, we chose a two time segments, with an example illustrated in Figure 1. While more time segments could be used, we found good convergence for these initial systems already with only two segments per transmon. The parameterized square pulse is given by,

$$\Omega_k(t) = \begin{cases} c_1 & 0 \leq t \leq t_1 \\ c_2 & t_1 \leq t \leq T \end{cases}, \quad (9)$$

where $-20 \text{ MHz} \leq c_i \leq 20 \text{ MHz}$ are amplitudes constrained to typical driving strengths, t_1 is the switching time and t_f is the total pulse duration. This is one of the simplest possible parameterizations, taking a value of c_1 for a duration t_1 and a value of c_2 for a duration $t_f - t_1$. Each transmon drive term also has a frequency modulation of the form $\exp(i\nu_k t)$, for a driving frequency ν_k , constrained to $(\omega_k - 2\pi \text{ GHz}) \leq \nu_k \leq (\omega_k + 2\pi \text{ GHz})$, where ω_k, ν_k are in units of $2\pi \text{ GHz}$. Therefore, the pulse parameters to optimize includes c_j, t_j and ν_k . With N transmons and j number of square pulses on each transmon, we then have $2Nj$ number of parameters to optimize. The pulse parameter optimizations were performed using l-BFGS-b.

We note that a recent preprint was just posted which uses similar quantum control considerations to improve VQE.⁴² However, in that work, the quantum control considerations are used to define an improved gate-based ansatz, unlike the direct variational pulse shaping described in this work.

ω_1	ω_2	δ_1	δ_2	g
4.8080	4.8333	0.3102	0.2916	0.0183

TABLE I: Device parameters appearing in Equation 3. All units are $2\pi \text{ GHz}$.

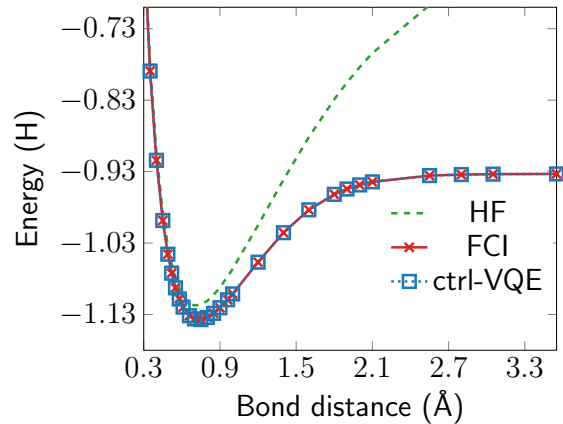


FIG. 2: Bond dissociation curve of H_2 molecule. ctrl-VQE energies computed using square pulses.

III. COMPUTATIONAL DETAILS

The numerical results presented in this work were generated with locally developed programs using functionalities from Qiskit and Qutip. Molecular integrals were generated using PySCF and STO-3G basis set was used throughout. The parameters ω, δ and g appearing in the two transmon qubit Hamiltonian, Equation 3, are explicitly given in Table I. To demonstrate qualitative insensitivity to the device parameters, we provide some results using a device with a larger detuning in the SI.

IV. RESULTS AND DISCUSSION

In the following subsections, we explore the ability of ctrl-VQE to reproduce Full Configuration Interaction (FCI) (exact diagonalization) bond dissociation energy curves for two small example diatomic molecules with complementary electron correlation profiles. We then analyze the dependence of the pulse time on the molecule's electron correlation, followed by a comparison to a representative gate-based circuit. After reporting the new results, we discuss comparisons with related quantum algorithms.

A. Dissociation of diatomic molecules

Here, we demonstrate the performance of our approach by computing the ground state molecular electronic energy along the bond dissociation of the H_2 molecule and the HeH^+ molecular ion. Although small, these

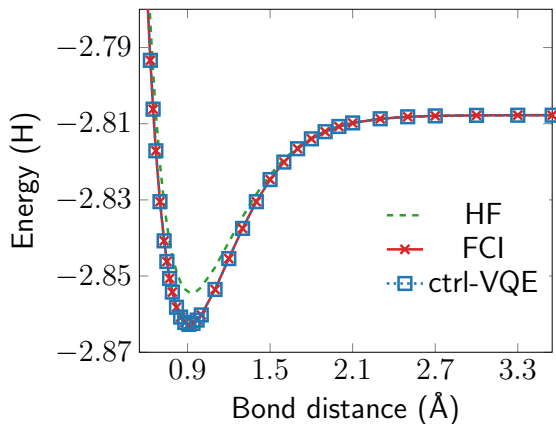


FIG. 3: Bond dissociation curve of HeH^+ molecule. **ctrl-VQE** energies computed using square pulses.

molecules have been used as benchmarks for quantum algorithms in the recent years.^{17,20,21,43–52} These two molecular examples are chosen because they present different behavior upon bond dissociation with respect to electronic structure of the molecules. As two-orbital, two-electron problems, these would naturally be modeled on four-qubits following the commonly used Jordan-Wigner transformation.²⁶ However, to make the pulse simulations more computationally efficient, we have used the parity mapping instead in which two qubits are diagonal and can be removed from consideration. Details are given in Ref.⁵³, and we use the implementation for mapping and pruning in Qiskit software.⁵⁴

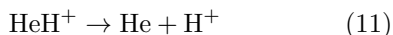
As a prototypical example of a homolytic dissociation,



Dynamic Correlation \rightarrow Static Correlation

as H_2 dissociates, the ground state moves from being dominated by a single Slater determinant to increasingly multiconfigurational, due to the shrinking HOMO-LUMO gap. As a result, the accuracy of a mean-field treatment (Hartree-Fock, HF) diminishes as the bond length is stretched. A comparison of HF with FCI and **ctrl-VQE** is shown for H_2 in Fig 2. It can be seen that **ctrl-VQE** reproduces the FCI energy with very high accuracy.

In stark contrast, HeH^+ becomes easier to model as the bond distance increases. The reason is that, being the strongest acid and, interestingly, the first molecule formed in the universe,⁵⁵ dissociation is a heterolytic deprotonation,



Dynamic Correlation \rightarrow No Correlation*

such that both the reactants and the products are both closed shell and well represented by a single Slater determinant. In fact, in a minimal basis set (i.e., the STO-3G basis set used in this paper), the products have exactly

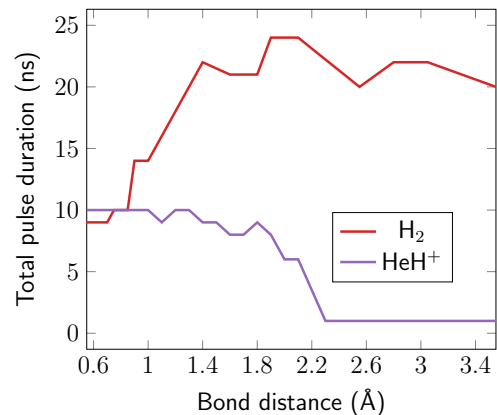


FIG. 4: Total pulse duration as a function of bond distance of H_2 and HeH^+ molecular systems. Square pulses were used to generate the **ctrl-VQE** molecular energies in Figs. 2 and 3. The shortest pulse duration at each geometry is plotted here.

zero electron correlation energy because the H^+ ion has no electrons, while the He atom has no empty virtual orbitals into which electrons can be promoted. As a result, Hartree-Fock becomes exact at dissociation. Of course, in larger basis sets, the He atom would have some dynamic correlation, hence the * in Eq. 11. The analogous HeH^+ curves are shown in Fig. 3.

Consistent with the physical descriptions above, Figs. 2 and 3 illustrate the Hartree Fock (HF) state moving quickly away from the FCI ground state with bond dissociation of H_2 , while the opposite is true for HeH^+ , as the HF state gradually converges to the exact FCI ground state with increasing bond distance.

The dissociation curves of H_2 and HeH^+ molecular systems produced with **ctrl-VQE** using the simple square pulses are also presented in Figures 2 and 3 respectively. **ctrl-VQE** reproduces the FCI bond dissociation curve of H_2 and HeH^+ with high accuracies. The maximum difference from the FCI energy along the dissociation curve is .03 mHa for both H_2 and HeH^+ , and the average error is .002 mHa in both the cases. More detailed information including the pulse parameters, characteristics and molecular energies along the dissociation curves are provided in the supplementary information. The resulting states have a good overlap with the exact FCI ground states (99% in all cases). For H_2 , it is possible for the overlap to deviate at far bond distances due to degenerate singlet and triplet states. As the bond distance increases, the singlet ground state of H_2 becomes degenerate with the lowest triplet state, making it possible to generate a superposition of a singlet and triplet. It is possible to converge to the exact ground singlet state by supplementing the objective function with a penalty term proportional to the total spin-operator (see SI for details).

B. Effect of electron correlation on pulse duration

In any VQE, one is typically interested in finding a useful balance between accuracy (needing deep circuits) and noise (needing shallow circuits). As such, molecular simulations of strongly correlated molecules are intrinsically more difficult as deeper circuits are required, which increases problems from noise and gate errors. An analogous balance is targeted in `ctrl-VQE`, where one would hope to obtain sufficiently accurate results with as short of a pulse time as possible. Because entanglement cannot be created instantly,⁴¹ we expect molecules with strong correlation to require longer pulses than simpler molecules.

In order to examine this relationship, in Fig. 4 we plot the duration of the shortest pulses we were able to obtain at each molecular geometry, with H_2 (HeH^+) shown in red (purple). Referring back to Eqs. 10 and 11, one would expect that as the bond distance is increased, H_2 , needing more entanglement, would in turn require increasing pulse durations, whereas pulses for HeH^+ would get increasingly fast as the bond is stretched. This trend is indeed observed.

The total pulse duration significantly decreases for the dissociation of the HeH^+ molecular ion, whereas it significantly increases, for the H_2 molecule. Note that the initial state and the final target state for HeH^+ becomes degenerate with increasing bond distance (above 2.0 Å). Thus, the Hartree Fock state ($|01\rangle$) is a good approximation to the exact FCI ground state, and only a slight modification to the initial state is required to well approximate the ground state. With `ctrl-VQE`, the total pulse duration at the far bond distances of HeH^+ are only 1.0 ns. This directly reflects the efficiency of the method presented in this work. In a gate-based compilation method, generally one would still construct an ansatz built up in terms of costly two-qubit gates, even though the target state is very nearly approximated by the initial state.

The total pulse duration at the dissociation limit for H_2 is significantly longer than near the equilibrium bond distance. Although the initial state monotonically increases with the increasing bond length, the same is not observed for the pulse duration. This is suggestive of the pulse durations reflecting the different dynamics along the bond dissociation of the two molecular systems (see SI for a more detailed analysis).

C. Comparison to gate-based ansätze

Now we directly compare the results of our pulse-based technique with gate-based variational ansätze. We use calibration data from an IBMQ device (mock Johannesburg device available in Qiskit software⁶⁷) to compute the duration of the circuits used to prepare trial wavefunctions. We consider the RY and UCCSD ansätze, which are capable of producing the exact ground state.

Here, the RY ansatz requires 1 CNOT, and the UCCSD

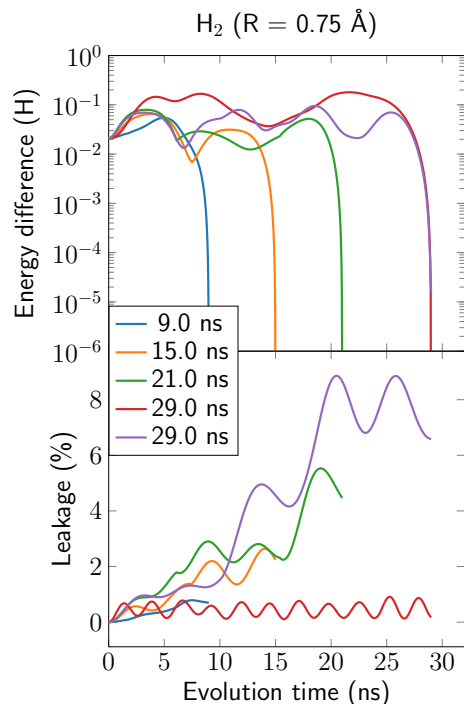


FIG. 5: Energy difference between `ctrl-VQE` and FCI (top) and leakage (bottom) along the time evolution steps with optimal pulses of different durations for H_2 with a bond distance of 0.75 Å. The red and purple lines with $T = 29$ ns, are distinct solutions to the same optimization. Optimized pulse parameters are provided in the SI.

requires 2 CNOTs. The RY ansatz has 4 parameters, and the UCCSD ansatz has 3 parameters. The total pulse time of the RY ansatz is 519 ns, and the UCCSD ansatz is 825 ns. In each case, the time to execute the circuit is significantly longer than the time required to apply the pulses using our pulse-based technique.

We note here that this comparison above needs to be approached with a bit of caution as our simulated device has slightly different parameters than the IBM-Q devices used for the circuit timings. However, we don't expect that our results would change that significantly if we had access to the full set of exact parameters of the device (including anharmonicities, bus frequencies, and couplings), because previous works using the present device parameter regime^{56,57} have demonstrated universal gate sets with single and two-qubit operations commensurate with those of the IBM-Q devices. As such, we expect the `ctrl-VQE` pulse times reported in this study to be within the same ballpark with what one would get by directly running the calculations on IBM-Q devices.

D. Time evolution with pulses

In Figs. 5 and 6, we track the evolution behavior of the calculation for various choices of the hyper-parameter, T ,

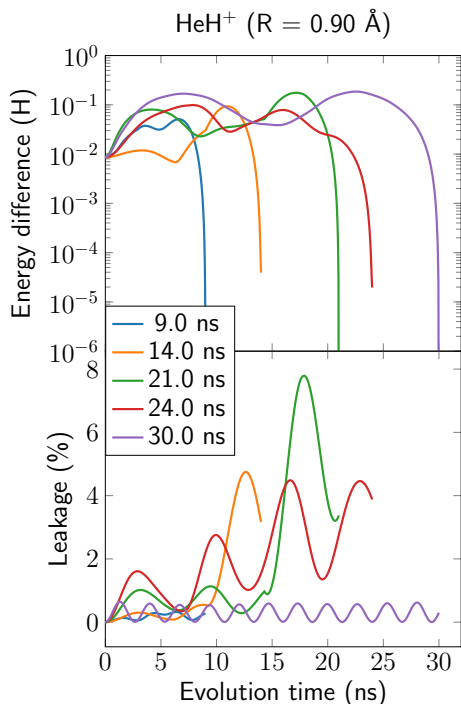


FIG. 6: Energy difference between ctrl-VQE and FCI (top) and leakage (bottom) along the time evolution steps with optimal pulses of different durations for HeH^+ with a bond distance of 0.90 Å. Optimized pulse parameters are provided in the SI.

(the total evolution time). In each of the two figures, the top panel displays the path the molecular energy takes as the state evolves from the reference Hartree-Fock state to the converged trial state, and the bottom panel displays the total population of the state outside of the $|0\rangle$ and $|1\rangle$ computational states for each qubit (“leakage”).

We see that for each value of T , the molecular energy of both H_2 and HeH^+ never decreases toward the exact energy monotonically, but rather increases initially, and then either decreases or oscillates before rapidly converging to the exact energy. While each of the optimized pulses do indeed generate suitable transmon dynamics which accurately produce the molecular ground state at specified time T , the different pulses are not each equally favorable. Considering the “leakage” in the bottom panels, we see that some pulses create much more leakage than other pulses. High levels of leakage will likely require a larger number of shots (pulse executions) to get precise determinations of the expectation values, since a higher portion of the shots end up in excited states which are either discarded, or collected for normalizing the results. However, with leakage of only 10%, we anticipate only needing a commensurate increase in the shot count to compensate for post-selection, and so we don’t expect this to be a fundamental limitation of the approach. Alternatively, one can use an unnormalized energy in the objective function. This approach naturally constrains

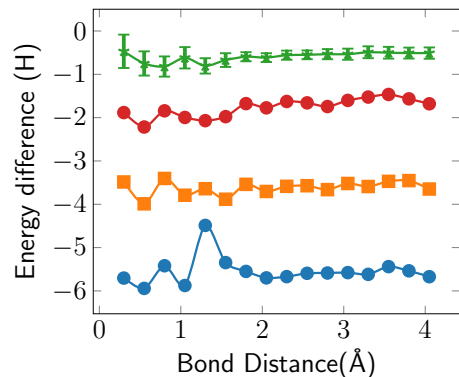


FIG. 7: Energy error for the dissociation of H_2 . Instead of using the exact, optimized parameters, we use parameters which have added Gaussian noise uncertainty. For each optimal parameter, we randomly sample 100 points each from a Gaussian distribution centered on its optimal setting and with a standard deviation of $\sigma = \{10^{-4}, 10^{-3}, 10^{-2}, 10^{-1}\}$ which correspond to the blue, orange, red and green curves respectively. The resulting energies for these 100 trials are then averaged. Error bars are given for each point but are smaller than some markers.

the solutions to simultaneously minimize leakage, as any leakage necessarily penalizes the associated pulse. Results using an unnormalized energy in the objective function are comparable to those shown here, and are given in the Supplementary Information.

E. Noise analysis

All the analysis thus far as been with the assumption of perfect control over the driving parameters used to generate an optimal state for the approximation of the ground state of chemical Hamiltonians. However, there are always uncertainties when attempting to implement the suggested driving parameters. In Fig. 7 we simulate the effect of the imprecise implementation of the optimal drive parameters. For each set of optimal drive parameters found by the ctrl-VQE protocol, we obtain 100 energy samples when using a noisy version of these parameters. To determine the noisy version of these parameters, we construct a Gaussian distribution with mean fixed to the optimal parameter value and a chosen standard deviation. For each parameter, we randomly select a noisy parameter following,

$$\theta_n \leftarrow \exp\left(-\frac{(\theta - \theta_o)^2}{2\sigma^2}\right), \quad (12)$$

where θ_n is a noisy version of the optimal parameter θ_o . In this way, the 100 energy samples will be calculated with random parameters which lie nearby the optimal ones, but without assumed infinite precision. We then average these 100 samples and find the resulting energy difference from the target ground state energy. With the

applied noise model, we can see that even imprecise settings can still be used to achieve accuracies below a 10^{-4} energy error. As shown in the red and green curves in Fig. 7, only when errors reach a magnitude of 10 MHz or 1 ns do the energy differences become significant enough to hinder the optimality of the suggested `ctrl-VQE` protocols. Since these errors are of the same order as the parameters themselves, they are of not a hindrance to the realistic implementation of `ctrl-VQE`. We do not include any explicit noise due to finite decoherence (T_1) or dephasing (T_2^*) since the pulses we find are many orders of magnitude shorter than the typical time scales for these effects.⁴⁰ As a confirmation of this assumption we modified our simulation to that of solving a Lindblad form master equation which includes these effects. Our objective function did not change significantly due to our short time scales.

F. Comparison with Circuit Compilation Techniques

Although several ansätze have been proposed to achieve shorter circuits, even the most compact approaches involve too many gates to implement on current hardware for reasonably large molecules. In order to reduce the time spent during the state-preparation stage, and thus the coherence time demands on the hardware, circuit compilation techniques have been designed to take a given quantum circuit and execute it either with fewer gates or by reoptimizing groups of gates for faster execution.

To execute the gate-based VQE (described in Section II A) experimentally, the gates in a circuit are compiled to the hardware level resulting in sequences of analog control pulses, using a look-up table that maps each elementary gate to the associated predefined analog pulse. The sequence of control pulses corresponding to the elementary gates in the quantum circuit are then simply collected and appropriately scheduled to be executed on the hardware. As such the compilation is essentially instantaneous, making the gate-based compilation technique well suited for VQE algorithms where numerous iterations are performed.

From a compactness perspective however, this gate based compilation is far from ideal, resulting in total pulse durations which are much longer than what might be obtained with optimized compilation techniques. As obvious from the one-to-one translation of gates to pulses, the overall circuit structure is not considered (or exploited) in gate-based compilations. Thus one may naturally be inclined to seek an optimal pulse sequence for the entire circuit. This has motivated compilation algorithms where control pulses are optimized for the target circuit, using numerical optimal control techniques such as gradient ascent pulse engineering (GRAPE)⁵⁸ for partially optimal compilation.⁵⁹ However, because the GRAPE algorithm itself is highly non-trivial, the compilation la-

tency for each iteration is of critical concern. Two of the GRAPE-based techniques are briefly described below, see Ref. 59 for a detailed discussion.

The GRAPE compilation technique employs an optimal control routine which compiles to the machine-level sequences of analog pulses for a target quantum circuit. This is achieved by manipulating the sets of time-discrete control fields that are executed on the quantum system. The control fields in the optimal routine is updated using gradients (see Ref. 60 for use of analytical gradients) of the cost function with respect to the control fields. The cost function here can simply be the fidelity, control pulse parameterization or the pulse time, for example. GRAPE compilation achieves significant speedups, 2-5x as compared to standard gate-based compilation. However, such speedup comes with a substantial cost even with the state-of-the-art computations. This amounts to long compilation latency and thus is unfit for practical use in VQE algorithms where several iterations are performed over the circuit parameters optimizations. The GRAPE-based compilation also suffers from the limitation of circuit size that it can handle⁶¹⁻⁶³.

On the other hand, partial compilation techniques achieves significant pulse speedups by leveraging the fast compilation of standard gate-based techniques and the pulse speedups of GRAPE-based compilations. Two flavors of such an approach is reported in Ref. 59. Both the approaches divides the whole circuit into blocks of subcircuits. In the so-called strict partial compilation, the structure of quantum circuits used in quantum variational algorithms are exploited to only perform GRAPE-based compilation on fixed subcircuits that are independent of the circuit parametrization. The optimal pulses using the GRAPE compilation techniques for the fixed blocks are pre-computed and simply concatenated with the control pulses from the gate-based compilations for the remainder blocks of the circuit. Thus, the compilation speed is comparable to the gate-based compilations in each iteration, but this method also takes advantage of pulse speedups from GRAPE-based compilations. As one may expect, the pulse speedups heavily depend on the circuit depth of the fixed blocks.

In the other flavor, flexible partial compilation, circuits are blocked into subcircuits, each with a single parameter to optimize in the quantum variational algorithm which ensures low depth of the subcircuit blocks. Hyperparameter optimizations are performed for each subcircuit, and they are utilized to find optimal pulses for the circuit blocks. It is noteworthy to mention that in the flexible partial compilation, compilation latency is reduced significantly (around 80x, see Ref. 59) by tuning the hyperparameters of the circuit blocks to speed up the convergence of optimal control in GRAPE. Flexible partial compilations achieve significant pulse speedups as compared to strict partial compilations. However, in spite of the high pulse speedups, the flexible partial compilation technique still diverges from the extremely fast compilation time of the standard gate-based methods. Thus,

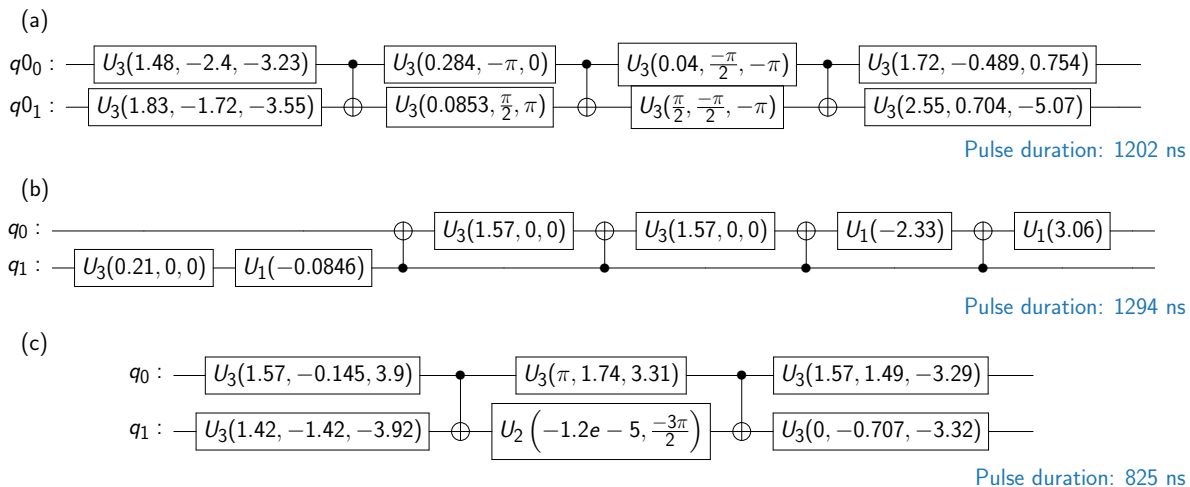


FIG. 8: Illustration of circuits constructed using the unitary and state vectors from `ctrl-VQE`. (a) Circuit corresponding to unitary obtained from a KAK decomposition. (b) An arbitrary circuit corresponding to the state vector. (c) Transpiled version of circuit (b).

the algorithm still suffers from compilation latency, although it is significantly reduced from the corresponding GRAPE-based compilation.

Although both of these GRAPE-based compilation techniques and `ctrl-VQE` share a direct pulse shaping step, they fundamentally differ because `ctrl-VQE` is not a compiler. In contrast to full or partial compiling, we make no reference to a circuit or implementing any specific unitary. Of course, the control pulses we find do implement *some* equivalent circuit or unitary (and we analyze these in Sec. IV G), but we have no need to specify this upfront. In fact, because `ctrl-VQE` only targets a single state, a large family of unitaries (defined by the behavior in the spaces orthogonal to the initial and final states) exist which minimize our objective function. As such, many possible solutions exist, with no immediate preference given to any one.

G. Decompile control pulses

In the previous sections, the efficiency of `ctrl-VQE` using optimized control pulses at the device level was demonstrated. The short pulse durations imply that applications to larger molecules might have even more significant speed up since the number of CNOTs in most VQE ansätze increases quickly.

Although `ctrl-VQE` is performed using no state preparation circuit, the unitary created by the time dynamics of the applied pulse *can* be decomposed into gates, allowing one to analyze the circuit. This is essentially running a compiler in reverse, or “decompiling” the pulse to yield a state preparation circuit. With this decompiled circuit in hand, we can evaluate the time it would take to execute the optimized pulse as a traditional circuit. By comparing this time to that of the pulse duration, one has a clean

benchmark for quantifying the overhead associated with gate-based state preparation. This decompilation can be done in two ways. In the first approach, we simply evolve the identity matrix (in the computational basis) by the optimized `ctrl-VQE` pulse. The evolved matrix is the matrix representation of the unitary generated by the pulse. A quantum circuit is then constructed using the KAK decomposition technique. For a detailed description of the technique, we refer the reader to Ref. 64.

In the second approach, an arbitrary circuit corresponding to the state vector from `ctrl-VQE` is constructed and then transpiled to obtain a shorter circuit depth. Using an IBMQ hardware (mock Johannesburg device available in Qiskit software), control pulses corresponding to the logic gates were obtained. The KAK decomposition, arbitrary circuit construction, transpilation and the mock circuit compilations were performed using Qiskit software⁵⁴. The quantum circuits are illustrated in Figure 8.

The corresponding pulse durations were 1202 ns for the circuit obtained using KAK decomposition and 825 ns for the circuit obtained from transpilation. The state vector used in this study was for the H_2 molecule at 0.75 Å and the corresponding pulse duration was 9 ns with `ctrl-VQE`. This clearly demonstrates the unnecessary circuit depths used for state preparation in the variational algorithm for the molecular system.

V. SUMMARY AND FUTURE OUTLOOK

We have presented a new quantum variational algorithm which is fundamentally different from the existing quantum algorithms for molecular simulation. The quantum circuit used for state preparation in standard variational algorithms is entirely replaced by a hardware-

level control routine with optimized pulse shapes to directly drive the qubit system. The efficacy of the presented method is numerically demonstrated by modelling the bond dissociation of two diatomic molecules, H_2 and HeH^+ . The maximum error from the exact FCI energy was well within chemical accuracy (0.02 kcal/mol) in both the molecular systems along the bond dissociation. `ctrl-VQE` captures the important electron correlation effects involved in the bond dissociation of the two molecular systems which is reflected in the pulse durations along the bond dissociation. The approach yields significant state-preparation speedups for VQE as compared to standard gate-based ansätze. The short pulse duration thereby naturally minimizes the loss due to decoherence and dephasing, which is a step toward enabling more accurate VQE simulations on larger, strongly correlated systems. The presented algorithm can be considered to be a lowest-level quantum variational algorithm.

Because the algorithm operates directly on the hardware, numerical simulations modeling the possible experiments are even more computationally expensive than typical VQE emulations, as one needs to not only solve the time-dependent Schrödinger equation, but also optimize the driving Hamiltonian. As such, the systems we

have been able to study so far are very small. In future work, we will develop an improved implementation to study the behavior of larger systems and with more sophisticated constraints on the pulse shape ($\Omega_n(t)$). Note that the high computational cost mentioned above is only present on these classical simulations which are modeling a `ctrl-VQE` experiment. These costs are completely absent from the experimental side, and we are currently working on an experimental implementation on custom hardware.

VI. ACKNOWLEDGEMENTS

O.R.M., N.J.M., S.E.E., and E.B. are grateful for financial support provided by the U.S. Department of Energy (Award No. DE-SC0018326). S.E.E and B.T.G acknowledge support provided by the U.S. Department of Energy (Award No. de-sc0019199). This work was done in part while N.J.M. was visiting the Simons Institute for the Theory of Computing. The authors thanks the Advanced Research Computing at Virginia Tech for the computational infrastructure.

* These two authors contributed equally

† Electronic address: nmayhall@vt.edu

¹ S. R. White, *Physical Review Letters* **69**, 2863 (1992).

² G. K.-L. Chan and M. Head-Gordon, *J. Chem. Phys.* **116**, 4462 (2002), ISSN 0021-9606.

³ U. Schollwöck, *Annals of Physics* **326**, 96 (2011).

⁴ B. Huron, J. P. Malrieu, and P. Rancurel, *J. Chem. Phys.* **58**, 5745 (1973), ISSN 00219606, URL <http://link.aip.org/link/?JCPSA6/58/5745/1>.

⁵ C. F. Bender and E. R. Davidson, *Phys. Rev.* **183**, 23 (1969), URL <https://link.aps.org/doi/10.1103/PhysRev.183.23>.

⁶ R. J. Buenker, *J. Chem. Phys.* **49**, 5381 (1968), ISSN 00219606.

⁷ S. Evangelisti, J.-P. Daudey, and J.-P. Malrieu, *Chemical Physics* **75**, 91 (1983), ISSN 0301-0104.

⁸ N. M. Tubman, J. Lee, T. Y. Takeshita, M. Head-Gordon, and K. B. Whaley, *J. Chem. Phys.* **145**, 044112 (2016), ISSN 0021-9606.

⁹ J. B. Schriber and F. A. Evangelista, *The Journal of Chemical Physics* **144**, 161106 (2016).

¹⁰ A. A. Holmes, N. M. Tubman, and C. J. Umrigar, *Journal of Chemical Theory and Computation* **12**, 3674 (2016).

¹¹ D. S. Levine, D. Hait, N. M. Tubman, S. Lehtola, K. B. Whaley, and M. Head-Gordon, *J. Chem. Theory Comput.* **16**, 2340 (2020), ISSN 1549-9618.

¹² V. Abraham and N. J. Mayhall, arXiv:2002.03107 [cond-mat, physics:physics] (2020), 2002.03107.

¹³ M. Caffarel, T. Applencourt, E. Giner, and A. Scemama, in *Recent Progress in Quantum Monte Carlo* (American Chemical Society, 2016), vol. 1234 of *ACS Symposium Series*, chap. 2, pp. 15–46, ISBN 978-0-8412-3179-5.

¹⁴ V. Abraham and N. J. Mayhall, arXiv:2002.03107 [cond-

mat, physics:physics] (2020), 2002.03107.

¹⁵ A. Peruzzo, J. McClean, P. Shadbolt, M.-H. Yung, X.-Q. Zhou, P. J. Love, A. Aspuru-Guzik, and J. L. O’Brien, *Nature communications* **5**, 4213 (2014), ISSN 2041-1723 (Electronic) 2041-1723 (Linking).

¹⁶ K. Sharma, S. Khatri, M. Cerezo, and P. J. Coles, *New Journal of Physics* **22**, 043006 (2020), URL <https://doi.org/10.1088%2F1367-2630%2F22043006>.

¹⁷ A. Kandala, A. Mezzacapo, K. Temme, M. Takita, M. Brink, J. M. Chow, and J. M. Gambetta, *Nature* **549**, 242 (2017), URL <https://doi.org/10.1038/nature23879>.

¹⁸ W. J. Huggins, J. Lee, U. Baek, B. O’Gorman, and K. B. Whaley, arXiv:1909.09114 [physics, physics:quant-ph] (2019), 1909.09114.

¹⁹ J. Lee, W. J. Huggins, M. Head-Gordon, and K. B. Whaley, *J. Chem. Theory Comput.* **15**, 311 (2019), ISSN 1549-9618.

²⁰ B. T. Gard, L. Zhu, G. S. Barron, N. J. Mayhall, S. E. Economou, and E. Barnes, *npj Quantum Information* **6**, 1 (2020), ISSN 2056-6387.

²¹ G. S. Barron, B. T. Gard, O. J. Altman, N. J. Mayhall, E. Barnes, and S. E. Economou, arXiv:2003.00171 [quant-ph] (2020).

²² I. G. Ryabinkin, T.-C. Yen, S. N. Genin, and A. F. Izmaylov (2018).

²³ H. R. Grimsley, S. E. Economou, E. Barnes, and N. J. Mayhall, *Nat. Commun.* **10**, 3007 (2019), ISSN 2041-1723.

²⁴ H. L. Tang, V. O. Shkolnikov, G. S. Barron, H. R. Grimsley, N. J. Mayhall, E. Barnes, and S. E. Economou, arXiv:1911.10205 [quant-ph] (2020), 1911.10205.

²⁵ I. G. Ryabinkin, R. A. Lang, S. N. Genin, and A. F. Izmaylov, *J. Chem. Theory Comput.* **16**, 1055 (2020), ISSN 1549-9618.

- ²⁶ W. Jordan, P., *Z. Physik* **47**, 631 (1928), URL <https://doi.org/10.1007/BF01331938>.
- ²⁷ S. B. Bravyi and A. Y. Kitaev, *Ann. Phys.* **298**, 210 (2002), URL <https://doi.org/10.1006/aphy.2002.6254>.
- ²⁸ J. T. Seeley, M. J. Richard, and P. J. Love, *The Journal of Chemical Physics* **137**, 224109 (2012), <https://doi.org/10.1063/1.4768229>, URL <https://doi.org/10.1063/1.4768229>.
- ²⁹ R. J. Bartlett and M. Musiał, *Rev. Mod. Phys.* **79**, 291 (2007), URL <https://link.aps.org/doi/10.1103/RevModPhys.79.291>.
- ³⁰ M.-H. Yung, J. Casanova, A. Mezzacapo, J. McClean, L. Lamata, and E. Aspuru-Guzik, A. and Solano, *Scientific Reports* **4**, 3589 (2014).
- ³¹ M. Ostaszewski, E. Grant, and M. Benedetti, arXiv:1905.09692 [quant-ph] (2019), 1905.09692.
- ³² D. Chivilikhin, A. Samarín, V. Ulyantsev, I. Iorsh, A. R. Oganov, and O. Kyriienko, arXiv:2007.04424 [cond-mat, physics:quant-ph] (2020), 2007.04424.
- ³³ [1909.12410v1] *A Jastrow-type decomposition in quantum chemistry for low-depth quantum circuits*, <https://arxiv.org/abs/1909.12410v1>.
- ³⁴ W. J. Huggins, J. Lee, U. Baek, B. O’Gorman, and K. B. Whaley, arXiv:1909.09114 [physics, physics:quant-ph] (2019), 1909.09114.
- ³⁵ J. Lee, W. J. Huggins, M. Head-Gordon, and K. B. Whaley (2018).
- ³⁶ R. Babbush, N. Wiebe, J. McClean, J. McClain, H. Neven, and G. K.-L. Chan, *Physical Review X* **8**, 011044 (2018).
- ³⁷ V. Verteletskyi, T.-C. Yen, and A. F. Izmaylov, *The Journal of Chemical Physics* **152**, 124114 (2020), <https://doi.org/10.1063/1.5141458>, URL <https://doi.org/10.1063/1.5141458>.
- ³⁸ W. J. Huggins, J. McClean, N. Rubin, Z. Jiang, N. Wiebe, K. B. Whaley, and R. Babbush, arXiv:1907.13117 [physics, physics:quant-ph] (2019), 1907.13117.
- ³⁹ A. Zhao, A. Tranter, W. M. Kirby, S. F. Ung, A. Miyake, and P. J. Love, *Phys. Rev. A* **101**, 062322 (2020), URL <https://link.aps.org/doi/10.1103/PhysRevA.101.062322>.
- ⁴⁰ J. Koch, T. M. Yu, J. Gambetta, A. A. Houck, D. I. Schuster, J. Majer, A. Blais, M. H. Devoret, S. M. Girvin, and R. J. Schoelkopf, *Phys. Rev. A* **76**, 042319 (2007).
- ⁴¹ S. Deffner and S. Campbell, *J. Phys. A: Math. Theor.* **50**, 453001 (2017), URL <https://doi.org/10.1088/1751-8121/aa86c6>.
- ⁴² A. Choquette, A. Di Paolo, P. K. Barkoutsos, D. Sénéchal, I. Tavernelli, and A. Blais, arXiv:2008.01098 [quant-ph] (2020), 2008.01098.
- ⁴³ Y. Wang, F. Dolde, J. Biamonte, R. Babbush, V. Bergholm, S. Yang, I. Jakobi, P. Neumann, A. Aspuru-Guzik, J. D. Whitfield, et al., *ACS Nano* **9**, 7769 (2015), ISSN 1936-0851.
- ⁴⁴ Y. Shen, X. Zhang, S. Zhang, J.-N. Zhang, M.-H. Yung, and K. Kim, *Phys. Rev. A* **95**, 020501 (2017), URL <https://link.aps.org/doi/10.1103/PhysRevA.95.020501>.
- ⁴⁵ J. I. Colless, V. V. Ramasesh, D. Dahlen, M. S. Blok, M. E. Kimchi-Schwartz, J. R. McClean, J. Carter, W. A. de Jong, and I. Siddiqi, *Phys. Rev. X* **8**, 011021 (2018), URL <https://link.aps.org/doi/10.1103/PhysRevX.8.011021>.
- ⁴⁶ A. J. McCaskey, Z. P. Parks, J. Jakowski, S. V. Moore, T. D. Morris, T. S. Humble, and R. C. Pooser, *npj Quantum Information* **5**, 1 (2019), ISSN 2056-6387.
- ⁴⁷ R. Xia, T. Bian, and S. Kais, *The Journal of Physical Chemistry B* **122**, 3384 (2018), pMID: 29099600, <https://doi.org/10.1021/acs.jpcc.7b10371>, URL <https://doi.org/10.1021/acs.jpcc.7b10371>.
- ⁴⁸ C. Hempel, C. Maier, J. Romero, J. McClean, T. Monz, H. Shen, P. Jurcevic, B. P. Lanyon, P. Love, R. Babbush, et al., *Phys. Rev. X* **8**, 031022 (2018), URL <https://link.aps.org/doi/10.1103/PhysRevX.8.031022>.
- ⁴⁹ K. Sugisaki, S. Nakazawa, K. Toyota, K. Sato, D. Shiomi, and T. Takui, *ACS Central Science* **5**, 167 (2019), <https://doi.org/10.1021/acscentsci.8b00788>, URL <https://doi.org/10.1021/acscentsci.8b00788>.
- ⁵⁰ M. B. Ritter, *Journal of Physics: Conference Series* **1290**, 012003 (2019), URL <https://doi.org/10.1088/2F1742-6596/2F1290/2F1/2F012003>.
- ⁵¹ R. Sagastizabal, X. Bonet-Monroig, M. Singh, M. A. Rol, C. C. Bultink, X. Fu, C. H. Price, V. P. Ostroukh, N. Muthusubramanian, A. Bruno, et al., *Phys. Rev. A* **100**, 010302 (2019), URL <https://link.aps.org/doi/10.1103/PhysRevA.100.010302>.
- ⁵² V. Armaos, D. A. Badounas, P. Deligiannis, and K. Lianos, *Applied Physics A* **126**, 625 (2020).
- ⁵³ S. Bravyi, J. M. Gambetta, A. Mezzacapo, and K. Temme, arXiv:1701.08213 [quant-ph] (2017).
- ⁵⁴ H. Abraham, AduOffei, I. Y. Akhalwaya, G. Aleksandrowicz, T. Alexander, E. Arbel, A. Asfaw, C. Azaustre, AzizNgoueya, P. Barkoutsos, et al., *Qiskit: An open-source framework for quantum computing* (2019).
- ⁵⁵ R. Güsten, H. Wiesemeyer, D. Neufeld, K. M. Menten, U. U. Graf, K. Jacobs, B. Klein, O. Ricken, C. Risacher, and J. Stutzki, *Nature* **568**, 357 (2019), ISSN 1476-4687.
- ⁵⁶ S. E. Economou and E. Barnes, *Phys. Rev. B* **91**, 161405 (2015), URL <https://link.aps.org/doi/10.1103/PhysRevB.91.161405>.
- ⁵⁷ G. S. Barron, F. A. Calderon-Vargas, J. Long, D. P. Pappas, and S. E. Economou, *Phys. Rev. B* **101**, 054508 (2020), URL <https://link.aps.org/doi/10.1103/PhysRevB.101.054508>.
- ⁵⁸ N. Khaneja, T. Reiss, C. Kehlet, T. Schulte-Herbrüggen, and S. J. Glaser, *Journal of Magnetic Resonance* **172**, 296 (2005), ISSN 1090-7807, URL <http://www.sciencedirect.com/science/article/pii/S1090780704003696>.
- ⁵⁹ P. Gokhale, Y. Ding, T. Propson, C. Winkler, N. Leung, Y. Shi, D. I. Schuster, H. Hoffmann, and F. T. Chong, *Proceedings of the 52nd Annual IEEE/ACM International Symposium on Microarchitecture* (2019), URL <http://dx.doi.org/10.1145/3352460.3358313>.
- ⁶⁰ S. Boutin, C. K. Andersen, J. Venkatraman, A. J. Ferris, and A. Blais, *Phys. Rev. A* **96**, 042315 (2017), URL <https://link.aps.org/doi/10.1103/PhysRevA.96.042315>.
- ⁶¹ D. Lu, K. Li, J. Li, H. Katiyar, A. Park, F. Jihyun, X. Guanru, L. Tao, L. Hang, B. Guilu, et al., *npj Quantum Information* **3**, 45 (2017).
- ⁶² T. Gradl, A. Spörl, T. Huckle, S. J. Glaser, and T. Schulte-Herbrüggen, in *Euro-Par 2006 Parallel Processing*, edited by W. E. Nagel, W. V. Walter, and W. Lehner (Springer Berlin Heidelberg, Berlin, Heidelberg, 2006), pp. 751–762, ISBN 978-3-540-37784-9.
- ⁶³ J. Cheng, H. Deng, and X. Qia, in *2020 ACM/IEEE 47th Annual International Symposium on Computer Architecture (ISCA)* (2020), pp. 543–555.
- ⁶⁴ C. P. Williams, *Explorations in Quantum Computing* (Springer, 2010).
- ⁶⁵ Or factorially, if a basis of Slater determinants is used to

span a target projected spin subspace.
⁶⁶ or a set of mutually commuting operators

⁶⁷ The mock Johannesburg device was taken from Qiskit Terra version 0.14.2